Wigner function modeling of resonant tunneling diodes with high peak-to-valley ratios

R. K. Mains and G. I. Haddad
Center for High-Frequency Microelectronics, Department of Electrical Engineering and Computer Science, The University of Michigan, Ann Arbor, Michigan 48109

(Received 8 January 1988; accepted for publication 2 August 1988)

Wigner function simulations of structures with experimentally observed high peak-to-valley ratios are carried out. It is shown that if care is taken with the numerical method used, the simulations reproduce these sharp resonances. When scattering is ignored, peak-to-valley ratios of 33.7 are obtained for a pseudomorphic InGaAs-AlAs structure. The effects of phonon scattering are included to first order. Also, a small-signal analysis is carried out and the results are used to predict the rf power generation capability of these devices.

I. INTRODUCTION

Estimates of the upper frequency limit for resonant-tunneling diodes[1–5] have indicated that these devices are useful into the THz range. Experimentally observed oscillation at 56 GHz[6] and detection of 2.5-THz signals[7] has generated considerable interest in the potential of these devices. The basic mechanism responsible for negative differential resistance and fast response times has recently been questioned in the literature.[5,8] It is therefore desirable to develop methods from quantum transport theory to model the transient behavior of resonant-tunneling devices.

The Wigner function method has been successful in modeling the general features of resonant tunneling diodes.[9,10] However, it has been found that this method underestimates the peak-to-valley ratios observed experimentally at low temperatures.[9] Also, simulations showing the high peak-to-valley ratios observed recently in InGaAs-InAlAs structures[11] have not yet been presented.

In this paper, a modified numerical method is used[12] which does predict high peak-to-valley ratios for these structures. Both the simulated peak-to-valley ratio and the peak current density are in the range of experimental results. Since agreement was not possible using the original numerical formulation of this method,[9,12] it is concluded that care is required in the numerical implementation of the problem.

The effects of phonon scattering have been included to first order in the modeling of GaAs-AlGaAs devices.[13] This article shows the effect of including InGaAs phonon scattering rates on device performance. Inclusion of phonon scattering at room temperature reduces the peak-to-valley ratio from 33.7 to 6.81.

An advantage of the Wigner function simulation method is that it readily allows modeling of transient and small-signal effects.[9,10] In this article, a small-signal analysis of an InGaAs-AlAs device is carried out. By assuming that the small-signal equivalent circuit of the device is constant over a given rf voltage magnitude range, an estimate of the rf power generation capability of the device is obtained.

The Wigner function method used is a single particle approach, i.e., many-body effects such as wave-function antisymmetrization and carrier–carrier scattering have not been included. The analysis is one dimensional with the assumption of a thermal equilibrium distribution for states in the transverse direction. Although the self-consistent field has been included in Wigner function simulations,[12] self-consistency has not been included in the results presented here.

II. BASIC METHOD AND EQUATIONS SOLVED

The equation for the time evolution of the Wigner function $f(x, k)$ is[14]

$$\frac{\partial f(x,k)}{\partial t} = -\frac{\hbar k}{m^*}\frac{\partial f(x,k)}{\partial x} + \left(\frac{\partial f(x,k)}{\partial t}\right)_c - \frac{1}{2\pi\hbar}\int_{-\infty}^{\infty} dk' \left\{2\int_0^{\infty} dy \sin([k-k']y) \times \left[V\left(x+\frac{y}{2}\right) - V\left(x-\frac{y}{2}\right)\right]\right\} f(x,k'), \quad (1)$$

where f is the one-dimensional Wigner function in m^{-2}, m^* is the effective mass in kg, and $V(x)$ is the potential energy for electrons in joules. In this equation, $(\partial f/\partial t)_c$ represents the time evolution of f due to scattering processes. To first order, scattering may be included in a manner similar to the scattering term appearing in the Boltzmann transport equation.[15] In the simulations including phonon scattering in this paper, a scattering term of the following form was included in the equations:

$$\left(\frac{\partial f(x,k)}{\partial t}\right)_c = -S_{\text{out}}(k) f(x,k) + \sum_{k'} S_{\text{in}}(k',k) f(x,k'), \quad (2)$$

where $S_{\text{out}}(k)$ is the scattering rate from the state with wave vector k to all other states, and $S_{\text{in}}(k',k)$ is the scattering rate into state k from another state k'. These scattering rates are calculated using the expressions from first-order perturbation theory,[16] considering bulk phonon modes only for acoustic and polar optic scattering. After proper normalization consistent with the one-dimensional Eq. (1), these expressions were evaluated numerically by summing over all k-space intervals included in the simulation to obtain the scattering rates of Eq. (2). The material constants appearing in the scattering expressions for InGaAs were obtained from Ref. 17.

 0021-8979/88/225041-04$02.40

The discretized form used to solve Eq. (1) is (for $k>0$)

$$\frac{f^f(x,k_m)-f(x,k_m)}{\Delta t}=-\frac{\hbar k_m}{m^*}\frac{f^f(x,k_m)-f^f(x-\Delta x,k_m)}{\Delta x}+\left(\frac{\partial f^f(x,k_m)}{\partial t}\right)_c+\frac{2}{\hbar N_k}$$
$$\times\sum_p\frac{\sin\{2\pi[(p-m)/N_k]\}}{2\pi[(p-m)/N_k]}\sum_{n=1}^{N_{\max}}\sin\left[\left(2n\pi\frac{p-m}{N_k}\right)\right][V(x+n\Delta x)-V(x-n\Delta x)]f^f(x,k_p)\,, \tag{3}$$

where m and p are indices indicating k and k', respectively, and where N_k is the number of k values included in the simulation. Equation (3) differs from previous discretizations[9,12] of Eq. (1) in the sin $(k)/k$ weighting, which effectively is a window that deemphasizes the high-frequency components in the discrete Fourier transform of the potential energy function. As is shown in Ref. 12, the effect of this weighting is to provide a more consistent approximation to the moment equations that are derived by multiplying Eq. (1) by k^n and integrating over all k space. In Eq. (3), the superscript f indicates that a quantity is considered to be at the future time, $t+\Delta t$; therefore, this is a fully implicit method. The upper limit in the Fourier transform of the potential energy, $N_{\max}$, is chosen so that Eq. (3) is numerically consistent with Eq. (1) for the linear potential case[12]; the value $N_{\max}=(2/3)N_k$ was used. For the simulations in this paper, $N_k=60$, $N_x=80$, and $N_{\max}=40$, where N_x is the number of mesh points in real space.

To obtain steady-state operating points on the I-V curve, Eq. (1) is solved for $\partial f/\partial t=0$, given a particular value of applied bias, which is assumed to be dropped uniformly across the double barriers and well. Starting from a particular dc solution, small-signal solutions are obtained by assuming a Wigner function of the form:

$$f(x,k)=f_{\rm dc}(x,k)+f_{\rm sms}(x,k)e^{i\omega t}. \tag{4}$$

Also, the potential energy becomes

$$V(x)=V_{\rm dc}(x)+V_{\rm sms}(x)e^{i\omega t}, \tag{5}$$

where $V_{\rm sms}(x)$ is applied across the double barriers and well only. Substituting Eqs. (4) and (5) into Eq. (3) and retaining first-order terms only yields a solution for the small-signal current density in the device. When the small-signal current density over the barrier and well regions is integrated and the ratio of the complex small-signal current and voltage phasors is taken, the admittance per unit area of the device is calculated. Since this admittance is due to the conduction current alone, the term $i\omega C$ is added to the admittance to account for the displacement current. The capacitance per unit area is determined from

$$C=\epsilon/W, \tag{6}$$

where W is the distance between the outer edges of the double barriers. For the structure analyzed in this paper, $W=90.4$ Å.

III. DEVICE STRUCTURE AND dc SIMULATION RESULTS

For the simulations, a pseudomorphic $In_{0.53}Ga_{0.47}As$-AlAs structure was chosen for which excellent experimental results recently have been reported.[11] Figure 1 shows the electron concentration and assumed potential energy for the dc, zero-bias solution of this structure. For this device, peak-to-valley ratios of 14 at room temperature and 35 at 77 K have been obtained experimentally, with peak current densities in the range of $2\text{–}4\times10^4$ A/cm^2. The conduction band discontinuity in Fig. 1 is assumed to be 1.2 eV, and the effective mass is assumed constant throughout the device and equal to 0.042 m_0, the InGaAs value.

Figure 2 shows the static I-V curve calculated at room

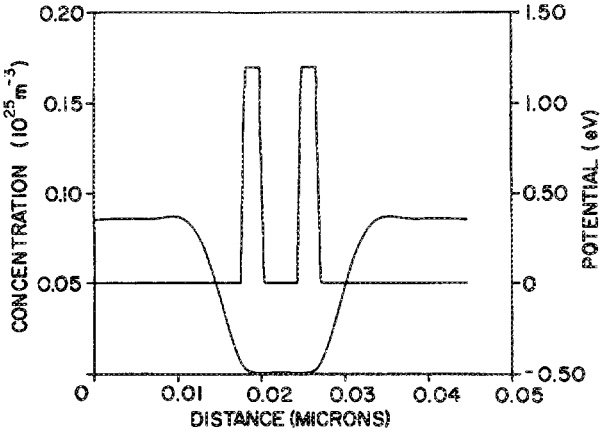

FIG. 1. Zero-bias solution for $In_{0.53}Ga_{0.47}As$-AlAs structure showing electron density and potential energy profile. Barrier width = 22.6 Å, well width = 45.2 Å.

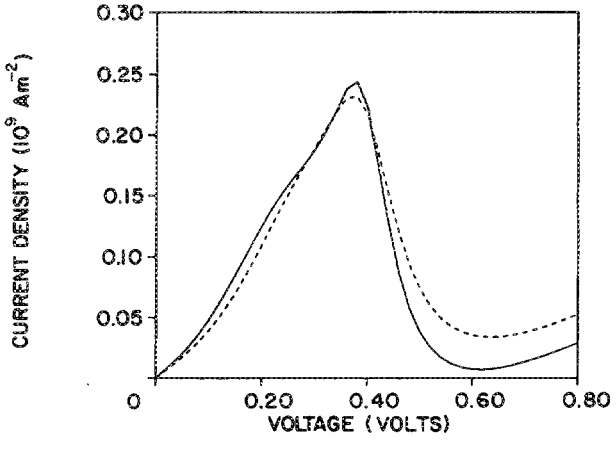

FIG. 2. Static I-V curve for the structure of Fig. 1 at room temperature both with (dotted curve) and without (solid curve) phonon scattering. Peak-to-valley ratio is 33.7 without scattering, 6.81 with scattering included. Numerical method of Eq. (3) was used.

temperature for this device, both with and without phonon scattering included. For the case without phonon scattering, a peak-to-valley ratio of 33.7 was calculated. When InGaAs scattering rates were used throughout the device, the calculated peak-to-valley ratio was 6.81. It is believed that this calculation underestimates the experimental peak-to-valley ratio due to uncertainties in the scattering rates as well as to numerical problems inherent to the solution of the Wigner function equations.[12] The calculated peak current densities with and without scattering were 2.31 and 2.43×10^4 A/cm^2, respectively, on the low end of the experimental current range.

In the experimental I-V curves, the peak and valley currents occur at higher voltages than the calculated values, at 0.7 and 1.0 V, approximately. It is believed that this discrepancy is due to the fact that self-consistency has not been included in these calculations. Preliminary work on Wigner function simulations including self-consistency[12] shows that approximately half the applied voltage can be dropped across accumulation and depletion regions adjacent to the device barrier regions.

For comparison, Fig. 3 shows the I-V curve for the case without scattering using the original numerical method.[9,12] This numerical method is obtained from the discretization given in Eq. (3) leaving out the $\sin(k)/k$ weighting. The peak-to-valley ratio obtained using this method was 2.57.

IV. SMALL-SIGNAL ANALYSIS AND ESTIMATED POWER GENERATION

To carry out the small-signal analysis, the device dc solution at $V_{dc} = 0.44$ V, $J_{dc} = 1.28\times10^4$ A/cm^2 was calculated, in the middle of the negative conductance region of Fig. 2. Figure 4 shows the electron concentration and potential energy profile for this solution, which corresponds to f_{dc} and V_{dc} in Eqs. (4) and (5). A small-signal voltage, V_{sms}, of different frequencies is superimposed on V_{dc} and is assumed to exist entirely across the barrier and well regions. All the small-signal calculations were carried out at room temperature and without phonon scattering.

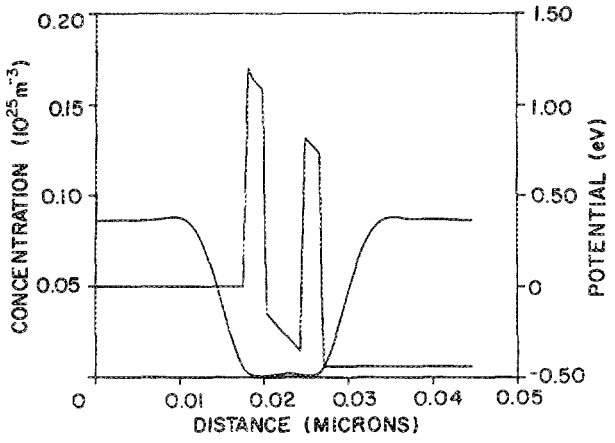

FIG. 4. dc solution at room temperature with $V_{dc} = 0.44$ V, $J_{dc} = 1.28\times10^4$ A/cm^2 for the case with no phonon scattering.

Figure 5 shows the real and maginary parts of the admittance calculated from the small-signal conduction current, as well as the ωC displacement current component. At low frequencies, G is just equal to the negative slope of the I-V curve in Fig. 2. From Figure 5, it is seen that the negative conductance of the device remains essentially constant up to a frequency of 3×10^{12} Hz. However, it is also seen that the ωC term in the admittance dominates above 10^{10} Hz so that the device capacitance limits the power generation capability at these frequencies.

The available rf power from this device as a function of frequency was estimated as follows. The small-signal admittance of Fig. 5 was assumed to remain constant over a large-signal voltage range of $(V_{rf})_{peak} = 0.1$V. The area of the device was chosen so that it is matched to 1-Ω circuit resistance, which requires that

$$A = -G/(G^2 + B^2), \tag{7}$$

where B is the total susceptance, i.e., the conduction plus displacement current parts. Again, since from Fig. 5 the ωC term dominates at high frequencies, the device area and rf power are limited by the device capacitance. The available rf power is given by

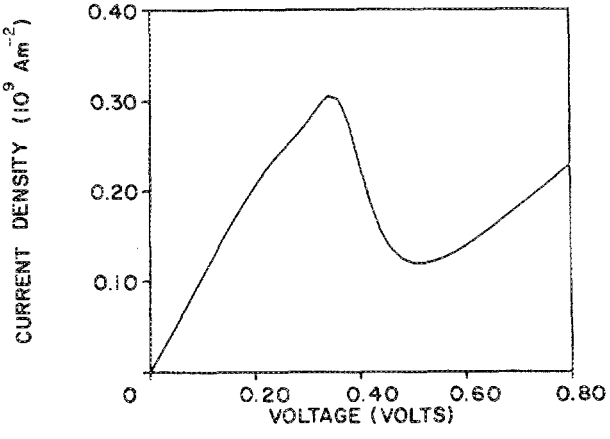

FIG. 3. Static I-V curve for the structure of Fig. 1 at room temperature and without scattering using the old numerical method [no weighting in Eq. (3)].

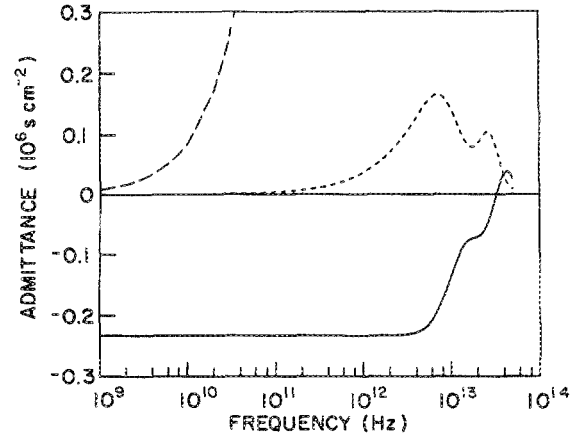

FIG. 5. Small-signal admittance calculated for the dc operating point at $V_{dc} = 0.44$ V in Fig. 4. Solid curve is Re(Y), small dashed curve is Im(Y), large dashed curve is ωC.

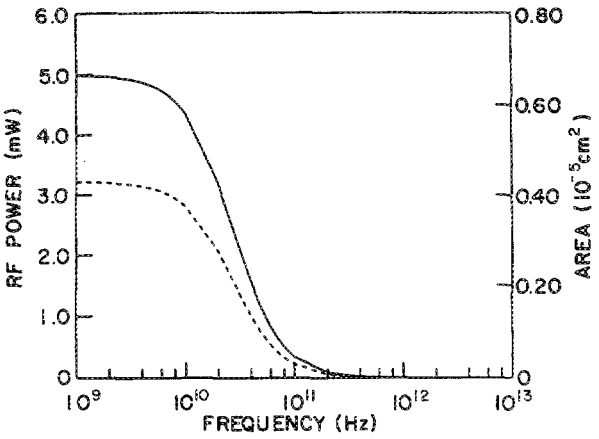

FIG. 6. Estimated power generation (solid) and device area (dashed) for 1-Ω matching based on the small-signal data of Fig. 5 and using $(V_{rf})_{peak} = 0.1$ V.

$$P_{rf} = [(V_{rf})^2_{peak}/2]/[1 + (B/G)^2] . \quad (8)$$

Figure 6 shows the estimated power generation capability of this device and the area required for 1-Ω matching. Note that these results assume no parasitic series resistance in the circuit, i.e., the circuit resistance is entirely made up of the 1-Ω load resistance R_L, that is absorbing power. If nonzero series resistance, R_s, exists in the circuit such that $R_s + R_L = 1\Omega$, the P_{rf} values in Fig. 6 would be scaled by the actual value of R_L.

The efficiency of the device may also be estimated as follows:

$$\eta = \frac{P_{rf}}{P_{dc}} = \frac{(-G)(V_{rf})^2_{peak}/2}{V_{dc}J_{dc}} = 8.88\times10^{-7}(-G) . \quad (9)$$

From Fig. 5, the negative conductance is essentially constant at the value 2.32×10^5 S/cm^2 up to 3×10^{12} Hz; putting this value in Eq. (9) yields a maximum efficiency of $\eta = 20.4\%$. At higher frequencies, η decreases as the negative conductance.

V. CONCLUSIONS

It has been shown that, if care is taken with the discretization of Eq. (1), it is possible to resolve sharp resonances in Wigner function modeling of resonant tunneling diodes. Both the calculated peak current density and peak-to-valley ratio are within experimental ranges, although inclusion of phonon scattering underestimates the experimental peak-to-valley ratio at room temperature. A small-signal analysis predicts that these devices should exhibit negative differential conductance up to frequencies of several THz, however device capacitance places a practical limit on device performance at several hundred GHz.

Further work needs to be done on refining the numerical method used to discretize Eq. (1). Also, self-consistency should be included in the simulation to bring the applied voltage values more in agreement with experimental results.

ACKNOWLEDGMENTS

This work was supported by the U.S. Army Research Office under the URI program, Contract No. DAAL03-87-K-0007. The authors wish to thank Dr. William Frensley for insightful discussions on quantum transport theory.

[1]B. Jogai, K. L. Wang, and K. W. Brown, Appl. Phys. Lett. **48**, 1003 (1986).
[2]D. D. Coon and H. C. Liu, Appl. Phys. Lett. **49**, 94 (1986).
[3]T. C. L. G. Sollner, E. R. Brown, W. D. Goodhue, and H. Q. Le, Appl. Phys. Lett. **50**, 332 (1987).
[4]D. S. Pan and C. C. Meng, J. Appl. Phys. **61**, 2081 (1987).
[5]T. Weil and B. Vinter, Appl. Phys. Lett. **50**, 1281 (1987).
[6]E. R. Brown, T. C. L. G. Sollner, W. D. Goodhue, and C. D. Parker, Appl. Phys. Lett. **50**, 83 (1987).
[7]T. C. L. G. Sollner, W. D. Goodhue, P. E. Tannenwald, C. D. Parker, and D. D. Peck, Appl. Phys. Lett. **43**, 588 (1983).
[8]S. Luryi, Appl. Phys. Lett. **47**, 490 (1985).
[9]W. R. Frensley, Phys. Rev. B **36**, 1570 (1987).
[10]W. R. Frensley, Appl. Phys. Lett. **51**, 448 (1987).
[11]T. Inata, S. Muto, Y. Nakata, S. Sasa, T. Fujii, and S. Hiyamizu, Jpn. J. Appl. Phys. **26**, L1332 (1987).
[12]R. K. Mains and G. I. Haddad (unpublished).
[13]W. R. Frensley, Solid-State Electron. **31**, 739 (1988).
[14]S. R. deGroot and L. G. Suttorp, *Foundations of Electrodynamics* (North-Holland, Amsterdam, 1972).
[15]J. Lin and L. C. Chiu, J. Appl. Phys. **57**, 1373 (1985).
[16]W. Fawcett, in *Electrons in Crystalline Solids* [International Atomic Energy Agency (IAEA), Vienna, 1973].
[17]S. R. Ahmed and B. R. Nag, Solid-State Electron. **28**, 1193 (1985).